High-Resolution Gamma-Ray Spectroscopy With a SiPM-Based Detection Module for 1" and 2" $LaBr_3$:Ce Readout

Giulia Cozzi, Paolo Busca, Marco Carminati, *Member, IEEE*, Carlo Fiorini, *Member, IEEE*, Giovanni L. Montagnani, Fabio Acerbi, *Member, IEEE*, Alberto Gola, *Member, IEEE*, Giovanni Paternoster, Claudio Piemonte, *Member, IEEE*, Veronica Regazzoni, *Member, IEEE*, Nives Blasi, Franco Camera, and Benedicte Million

***Abstract*— In this paper, we present a silicon photomultiplier (SiPM)-based photodetector module designed to readout large cerium-doped lanthanum bromide ($LaBr_3$:Ce) scintillators (cylindrical 1" × 1" and 2" × 2") for nuclear physics experiments. The detector prototype has a modular structure and implements a real-time stabilization of the SiPM gain to compensate for the gain drift with temperature. The SiPM module consists of an array of 5 by 6 near-ultraviolet high-density SiPMs (Fondazione Bruno Kessler, Italy), each one having an active area of 6 mm × 6 mm and 30-μm microcells. The single array is used for the 1" crystal readout, and it is assembled in a 2×2 format to read the 2" scintillator. Spectroscopic measurements were performed with both crystals. The 2" crystal was irradiated with different radioactive sources in an energy range between 122 keV and 1.3 MeV, and an energy resolution of 3.19 ± 0.01% full-width at half-maximum (FWHM) has been achieved at 662 keV. The result is very close to the 3.07 ± 0.03% FWHM measured with Super Bialkali photomultiplier tube (PMT) (Hamamatsu R6233-100) at the same energy with the same 2" crystal. In the framework of the comparison between SiPM and PMT for $LaBr_3$:Ce readout, we provide an analysis of the energy resolution contributions based on the measurements performed with the developed gamma-ray detection system.**

***Index Terms*— Cerium-doped lanthanum bromide ($LaBr_3$:ce), gamma-ray spectroscopy, nuclear physics, photomultiplier tube (PMT), silicon photomultiplier (SIPM).**

Manuscript received September 15, 2017; revised November 29, 2017; accepted December 12, 2017. Date of publication December 15, 2017; date of current version January 17, 2018. This work was supported by Italian INFN through the GAMMA Experiment.

G. Cozzi, M. Carminati, C. Fiorini, and G. L. Montagnani are with the Dipartimento di Elettronica, Informazione e Bioingegneria, Politecnico di Milano, 20133 Milan, Italy, and also with INFN, Sez. Milano, 20133 Milan, Italy (e-mail: carlo.fiorini@polimi.it).

P. Busca is with the Dipartimento di Elettronica, Informazione e Bioingegneria, Politecnico di Milano, 20133 Milan, Italy, with INFN, Sez. Milano, 20133 Milan, Italy, and also with ESRF, 38000 Grenoble, France.

F. Acerbi, A. Gola, G. Paternoster, and C. Piemonte are with Fondazione Bruno Kessler, 38123 Trento, Italy, and also with the Trento Institute for Fundamental Physics and Application, 38123 Trento, Italy.

V. Regazzoni is with Fondazione Bruno Kessler, 38123 Trento, Italy, with the Università degli studi di Trento, 38122 Trento, Italy, and also with the Trento Institute for Fundamental Physics and Application, 38123 Trento, Italy.

N. Blasi and B. Million are with INFN, Sez. Milano, 20133 Milan, Italy.

F. Camera is with INFN, Sez. Milano, 20133 Milan, Italy, and also with the Department of Physics, Università degli studi di Milano, 20133 Milan, Italy.

I. Introduction

THE recent availability of large and high-resolution inorganic scintillators like cerium-doped lanthanum bromide ($LaBr_3$:Ce) has raised a relevant interest in nuclear physics research where high-energy gamma-rays (from few tens of kiloelectron volts up to tens of megaelectron volts) are detected [1]. $LaBr_3$:Ce has some of the best scintillation properties among currently known scintillator materials for gamma-ray detection and spectroscopy. The properties of $LaBr_3$:Ce have been deeply investigated, showing a fast scintillation decay of 16 ns, a high light yield (more than 60 ph/keV), a high density (HD) of 5.08 g/cm^3, and the availability with large size (up to 3.8" × diameter 9.7" length) [2]–[5]. These features make $LaBr_3$:Ce a suitable and cost-effective alternative—or complementary solution—to high-purity germanium (HPGe) for high-energy gamma-ray detection, being also effective in reducing the Doppler broadening effect when it is larger than the intrinsic resolution of HPGe detectors [6]–[9].

$LaBr_3$:Ce crystals have been typically coupled to photomultiplier tubes (PMTs), achieving an energy resolution of 3% at 662 keV [10]–[13]. However, PMTs can suffer from several limitations in terms of mass and bulkiness, high biasing voltage, sensitivity to magnetic fields, fragility and, above all, nonlinearity when used in a wide energy range (from few tens of kiloelectron volts up to tens of megaelectron volts) [5], [11], [14]. The nonlinearity problem can be managed by reducing the biasing voltage or the number of dynodes [11], [15], [16]. Moreover, in applications where spectroscopy and imaging capability are both required, the use of a position-sensitive PMT is recommended for a good spatial resolution. However, these devices have the disadvantage of a higher nonlinear response with respect to spectroscopic-grade PMTs [17]–[19].

The recent improvements of solid-state photodetectors represent an attractive alternative to the consolidated PMT readout in the current state-of-the-art. Solid-state photodetector can overcome some important issues offering advantages like the compactness and the insensibility to magnetic fields, typical of silicon devices. Moreover, they can be assembled in arrays and tiles, enabling high-resolution spectroscopy and imaging with scintillators based on the Anger architecture in very compact

TABLE I
RESOLUTION PERFORMANCE OF $LaBr_3$:Ce READOUT WITH SIPMS

Ref.	Application	Crystal Size	SiPM Type	SiPM Active Area	Number of channels	Energy resolution
[35]	TOF PET	$3\times3\times5mm^3$	Hamamatsu (S10362-33-050C)	3×3 mm^2	1	3.2% (511keV)
[36]	TOF PET	$4\times4\times5mm^3$ $4\times4\times30mm^3$	FBK (NUV)	4×4 mm^2	1	6.6%; 7% (511keV)
[37]	Space	$6\times6\times10mm^3$	Hamamatsu (S10985-050C)	3×3 mm^2	4 (2×2 ch)	5.7% (662keV)
[38]	Space	$13\times13\times13mm^3$	Hamamatsu (S11828-3344)	3×3 mm^2	16 (4×4 ch)	4.5% (662keV)
[39]	Space	$16\times18\times5mm^3$	Hamamatsu (n.a)	3×3 mm^2	16 (4×4 ch)	6.5% (511keV)
[40]	TOF PET	$18\times16\times10mm^3$	Hamamatsu (S11064-050P)	3×3 mm^2	16 (4×4 ch)	6.4% (511keV)
[41]	Spectroscopy	1" × 1"	Hamamatsu (S10985-025C)	3×3 mm^2	4 (2×2 ch)	9.8% (662keV)
[42]	Spectroscopy	1" × 1"	Hamamatsu (S11827-3344MG)	3×3 mm^2	16 (4×4 ch)	5.3% (662keV)
[43]	Spectroscopy	1" × 1"	Hamamatsu (S12642-0808PA)	3×3 mm^2	64 (8×8 ch)	3.88% (662keV)
[44]	Space	$28\times28\times20mm^3$	SensL (MicroFB-60035)	6×6 mm^2	16 (4×4 ch)	4% (662keV)
This work	Spectroscopy	2" × 2"	FBK (NUV-HD)	6×6 mm^2	72	3.2% (662keV)

detection modules [20]–[23]. On the other side, solid-state photodetectors are a less consolidated technology than PMT, which are still widely used in many applications. Moreover, the leakage current and the possible crosstalk and afterpulse events are a more critical issue for solid-state photodetectors than for PMT.

There are different studies regarding the readout of $LaBr_3$:Ce with silicon drift detector (SDD), achieving the best energy resolution of 2.7% at 662 keV with a 5×5 mm^2 and 6×6 mm^2 crystal [12], [24]. A larger crystal of 1" × 1" was also tested in [25] showing a 3% energy resolution at the same energy. Finally, a 2" × 2" $LaBr_3$:Ce crystal was irradiated with different radioactive sources from 300 keV up to 1.8 MeV, achieving an energy resolution of 3.40% at 662 keV [26]. With respect to nonlinearity, SDD is not affected by this limitation. Although these results are close or even better than what achievable with standard PMTs, because of the high quantum efficiency (∼80%) and the absence of excess noise due to the absence of internal multiplication, SDD readout suffers from some limitations. In fact, the drift time typical of SDD limits its use with fast scintillators, in particular in nuclear physics experiments, where timing is required. Moreover, as described in [26], another problem is the high leakage current that mandatorily requires the implementation of a dedicated cooling strategy, to reduce its contribution to the energy resolution, which significantly increases the complexity of the detection module design.

In this context, silicon photomultipliers (SiPMs) are an emerging solid-state technology, considered a promising alternative to PMTs in many applications, as and medical imaging applications time-of-flight positron emission tomography (TOF-PET), single-photon emission computed tomography (SPECT), high-energy prompt gamma imaging, high-energy physics, and astroparticle physics thanks to their high gain, low-voltage operation, robustness, compact design and excellent timing performances [1], [20], [23], [27]–[34]. With respect to nonlinearity, SiPMs typically have a higher response nonlinearity than PMTs and this may be a limitation for high-energy applications. However, SiPM arrays with a very large number of microcells, such as used in this paper, can indeed have a wide dynamic range of linear response. Although SiPM technology is rapidly evolving and some efforts have been recently devoted to coupling these devices with large $LaBr_3$:Ce crystals, in the literature, to our knowledge, only a few results have been so far reported and the main works are summarized in Table I (sorted for increasing crystal size). The main application fields, which would benefit from this technological advancement, are in space science (gamma-ray telescopes, high-energy astronomy and solar physics, where 1" crystals were employed) and TOF-PET, where small crystals are characterized mostly in terms of timing resolution. An energy resolution of 3.2% has been measured at 511 keV in [35] with a small crystal. Considering large scintillators, the best energy resolution reported with the largest crystal of $28\times28\times20$ mm^3 size is of 4%, measured at 662 keV coupling the crystal to a SiPM array from SensL in a Compton telescope for gamma-ray astronomy [44].

The main challenges for large $LaBr_3$:Ce readout in nuclear physics are as follows:

1) the need for several units to cover the large area of detection, resulting in the introduction of dead areas which are due to array assembly and tiling;
2) the presence of a possible saturation effects due to high yield of $LaBr_3$:Ce in the energy range of these applications;
3) the issue of the gain instability with temperature variations, which is very important for such a high-resolution target.

Just recently, the technological improvements are making available devices with a microcell size smaller than 50 μm with the consequent reduction of the microcells recovery time, a photodetection efficiency (PDE) higher than 30%, and a dark count rate (DCR) lower than 1 Mcps/mm^2. These features are mandatory to improve the dynamic range and to achieve good spectroscopic results.

In this framework, the goal of this paper is to design and test a SiPM-based photodetector module for 1" up to 2" $LaBr_3$:Ce readout, with the introduction of a new SiPM

technology, which provides a high efficiency, a low noise, and a small microcell size. The module also implements a strategy to reach the thermal stabilization of the SiPM gain. The focus is on assessing the best energy resolution and providing a comparative study between SiPM- and PMT-based readout in terms of achievable performances, demonstrating their equivalence for high-resolution spectroscopy.

In Section II, we provide a theoretical analysis of the energy resolution of a gamma-ray system, useful for a comparison with PMT performances. Then, Section III provides a description of the prototype of detection module realized and designed to readout 1" × 1" and 2" × 2" $LaBr_3$:Ce crystals. In Section IV, we report spectroscopic results with the two scintillators. The 1" was tested between 122 and 662 keV, while the 2" was irradiated from 122 keV up to 1.3 MeV, achieving promising results in terms of energy resolution. Finally, in Section V we show a detailed comparative study between SiPM and PMT performances based on the theoretical analysis illustrated in Section II.

II. Energy Resolution

The energy resolution of a gamma-ray spectroscopy system based on scintillator R_{tot} at a given energy E can be described as the sum of three main contributions [13], [45], [46]

$$R_{\text{tot}} = \sqrt{R_{\text{intr}}^2 + R_{\text{stat}}^2 + R_{\text{noise}}^2}. \tag{1}$$

The first term of (1) indicates the intrinsic resolution of the scintillator and represents a limitation to the best achievable resolution for a given material. It is related to several effects, such as inhomogeneity due to local variations of the light yield in the scintillator, changes in the diffuser/reflector reflectivity, as well as nonproportionality of the scintillator response [47], [48].

The second term is the statistical contribution and it summarizes the generation of photoelectrons usually described by Poisson statistics, worsened by the excess noise factor (ENF) of the multiplication process, if any. It can be expressed as

$$R_{\text{stat}} = 2.355 \cdot \sqrt{\frac{\text{ENF}}{E \cdot Y \cdot \eta}}. \tag{2}$$

The denominator represents the average number of photoelectrons generated by the photodetectors. It depends on the energy E, on the scintillation yield (Y), as well as on the efficiency of the photoelectron conversion process η. The efficiency is dominated by the quantum efficiency η_q of the photodetector (PDE for SiPMs) and by the photon collection efficiency η_c due to the scintillator-photodetector optical coupling. For PMT, the statistical uncertainty of the signal is due to the variance of the electron multiplier gain ε and the ENF term is replaced by $1 + \varepsilon$.

The third contribution is related to the electronic noise of the readout chain and can be written as [46]

$$R_{\text{noise}} = 2.355 \cdot \sqrt{\frac{N \cdot \text{ENC}^2}{(E \cdot Y \cdot \eta \cdot q \cdot M)^2}} \tag{3}$$

where N is the number of photodetectors, q is the elementary charge, ENC is the equivalent noise charge in electrons root mean square for each photodetectors + electronics channel, and M is the multiplication factor of the photodetector. ENC is due to three main contributions to the noise: the parallel noise, i.e., the shot noise of the photodetector's leakage current, the series noise, and the $1/f$ noise of the input FET

$$\text{ENC}^2 = \text{ENC}_{\text{Parallel}}^2 + \text{ENC}_{\text{series}}^2 + \text{ENC}_{1/f}^2 \tag{4}$$

and the ENC can be optimized finding an optimum shaping time [49].

In case of multiplying photodetectors, such as SiPMs, readout by low-noise electronics, the dominant noise contribution is given by the shot noise due to DCR of SiPMs, which can be written as

$$\text{ENC}_{\text{Parallel}}^2 = 2 \cdot q^2 \cdot \text{DCR} \cdot A \cdot M^2 \cdot \text{ENF} \cdot \tau \cdot A_3 \tag{5}$$

where q is the elementary charge, A is the photodetector area, τ is the shaping time of the filter, and A_3 is the shaper constant [49]. Therefore, a high number of photoelectrons and low-noise electronics are mandatory features to achieve a high-resolution detection system. The number of photoelectrons can be enhanced by improving the efficiency, i.e., by choosing photodetectors with high PDE in the emission range of the scintillator, by reducing dead areas in the detector array assembly and by enhancing the fill factor (FF) of SiPMs' microcells. Moreover, a low value of DCR can keep the contribution of the electronics noise low enough, while increasing the area of the photodetector to readout large scintillators foreseen in the application. Moreover, a fast detector can allow using a short shaping time, decreasing the noise integration.

In this contest, we employ a new SiPM technology fabricated by Fondazione Bruno Kessler (FBK, Italy). As explained in Section III-B, it features a PDE = 45% at 380 nm, an FF = 77%, a cell density = 1100 cells/mm^2, a DCR < 100 kcps/mm^2, and recovery time ∼ 60 ns. These features make the tested technology competitive with other commercial detectors, which show PDE ∼ 40%, FF ∼ 75%, DCR ∼ 100 kcps/mm^2, and recovery time ∼ 50 ns [50]–[52].

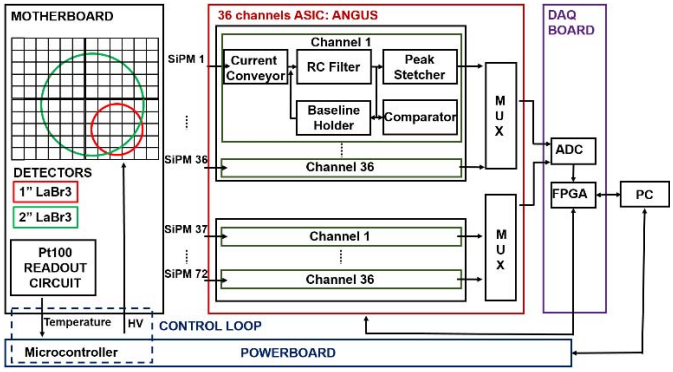

Fig. 1. Block scheme of the detection module for 1" and 2" $LaBr_3$:Ce readout.

III. Design of the Detection Module

The SiPM-based detection module was designed to have a modular structure and to be compatible for both 1" × 1" and 2" × 2" $LaBr_3$:Ce readout. Fig. 1 shows a block scheme of the main components of the detection system that can be grouped

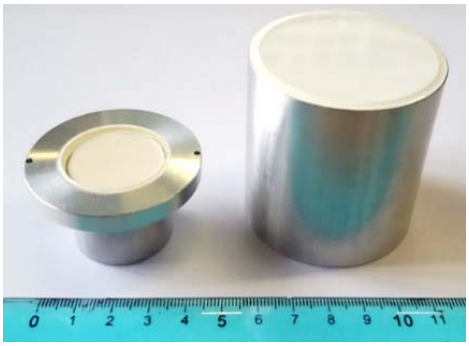

Fig. 2. Photograph of the 1" × 1" (left) and 2" × 2" (right) $LaBr_3$:Ce crystals characterized in this paper.

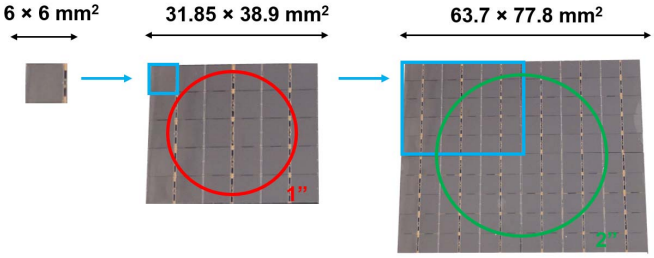

Fig. 3. (a) Basic element of the SiPM array: single NUV-HD SiPM with 6×6 mm^2 active area. (b) SiPM array of 31.85×38.9 mm^2 (5×6) for 1" $LaBr_3$:Ce readout. (c) Array of four SiPM tiles of total 63.7×77.8 mm^2 area for 2" $LaBr_3$:Ce readout.

in four sections: 1) scintillator; 2) SiPM array; 3) readout electronics; and 4) SiPM gain stabilization over temperature. A description of each block is provided in the following.

A. Scintillators

Cylindrical monolithic 1" × 1" (serial number: J146) and 2" × 2" (serial number: A7438Cs) $LaBr_3$:Ce (5% doped) from Saint Gobain are used (Fig. 2). They are prepackaged by the manufacturer, wrapped with reflectors, and sealed in an aluminum housing with a quartz optical window. Crystals are coupled to SiPMs (Section III-B) by means of BC-630 silicone optical grease from Saint Gobain that shows 95% of transmission in the 280–700 nm spectral range.

B. SiPM Array

The basic element of the array is a near-ultraviolet (NUV)- HD SiPM, fabricated by FBK, Italy, of 6 mm × 6 mm active area [Fig. 3(a)] and with 30 μm × 30 μm microcells. It is produced for NUV and blue light detection in HD technology. A full characterization of NUV-HD SiPMs is reported in [53].

This technology features a peak efficiency of 57% at 430 nm and an efficiency of 45% at 380 nm in the region of maximum emission of $LaBr_3$:Ce. As evident from (2), a high value of PDE provides a high average number of photoelectrons, which improves the statistical term in the energy resolution.

Moreover, the HD cell technology of FBK allows producing devices with small microcells size that improves dynamic range in high-energy applications, while, at the same time, featuring high FF at cell level and retaining a similar PDE of other devices with lower cell density [54]. The SiPMs used in this paper feature a microcells FF of 77%, which is already included in the quantum efficiency estimation (PDE = 45% at 380 nm), and a cell density of 1100 cells/mm^2. The dead areas between SiPMs composing one array and the dead gap between two or more SiPM arrays are included in the photon collection efficiency ($\eta_c = 70\%$), whose value has been estimated in this paper with the procedure explained in Section IV-B).

In addition, with reference to (5), the DCR < 100 kcps/mm^2 (overvoltage < 8 V) at 20 °C of this technology makes the noise contribution to the energy resolution negligible in an energy range from few hundreds of kiloelectron volts up to tens of megaelectron volts. In this energy range, the noise contribution remains still negligible even with the large area arrays necessary for large scintillators readout. An average DCR can be used in the parallel noise estimation with (5) instead of considering also the crosstalk on dark events, which turn out to be negligible, as detailed in Section IV-B.

Finally, NUV-HD SiPMs feature a microcells recharge time constant smaller than 100 ns, that allows using a short shaping time decreasing the noise integration (5) and preventing ballistic deficit [55].

The array of SiPMs, fabricated by FBK as well, is composed of 30 individual SiPMs arranged in 5 × 6 format [Fig. 3(b)] with a total area of 31.85 mm × 38.9 mm. The FF of the array assembly, which should be included in the photon collection efficiency of (2), is about 90%.

The SiPMs of the array are selected with a uniform breakdown voltage of 26.50 ± 0.15 V. Because of this small variability, in this paper the same biasing voltage is given to all the SiPMs without an evident worsening of spectroscopic results (the estimated SiPM gain spread is 0.4%, negligible with respect to the achieved energy resolution). This array is used for 1" × 1" $LaBr_3$:Ce readout. Only 25 SiPMs are coupled to the crystal, while the remaining five SiPMs are not connected to the electronics, but their presence improves the mechanical robustness of the tile.

This four-side buttable array is foreseen as basic unit for the assembly of larger arrays to read larger scintillators. For instance, in order to readout the 2" × 2" crystal, a total of four SiPM arrays are needed, arranged in 2 × 2 planar format with a total area of 63.7 mm × 77.8 mm [Fig. 3(c)]. Only 72 SiPMs are read by electronics. The remaining 48 SiPMs are not connected because of the limited available number of ASIC channels, as explained in Section III-C. For this reason and since the same electronics is used for 1" and 2" readout, the 2" is not centered in the 4 × 4 arrays assembly. Nevertheless, the 2" crystal surface is fully covered by these 72 SiPMs.

The modular structure was also designed to measure high-energy gamma-rays with a 3.5" × 8" $LaBr_3$:Ce, typically used in nuclear physics applications [56]. In that framework, a total of nine SiPM arrays will be arranged in 3 × 3 format.

C. Readout Electronics

SiPMs' signals are read by ANGUS, a 36-channel front-end ASIC in standard CMOS 0.35-μm technology developed for SPECT applications. Its detailed description can be found

in [57]. A single ASIC is used for the readout of 25 SiPMs coupled to the 1" × 1" $LaBr_3$:Ce, while two chips are needed for the 2" × 2" crystal readout. Because the chip was designed to acquire the energy spectra of the radiation sources typically used in SPECT, i.e., ^{99}Tc (140 keV), it shows a limited dynamic range for the energy range of nuclear physics experiments. For this reason, it was not possible to acquire energy gamma transitions higher than 1.33 MeV.

As schematically illustrated in Fig. 1, a single channel of the ASIC features first a current conveyor input stage. The current signal enters a programmable *RC* circuit which can filter the signal with eight shaping times ranging from 200 ns to 10 μs. The signal is sent at the same time to a peak stretcher and to a comparator. The comparator provides a trigger when the signal overcomes a threshold, programmable by an internal DAC. The peak stretcher stores the peak value as the trigger signal is generated. A baseline holder circuit is designed to set the baseline voltage to a fixed value, regardless of any undesired dc current coming from the current conveyor and of the event rate. The stored value is sent to an analog multiplexer, whose output is connected to Data AcQuisition (DAQ) board that is equipped with a differential 12-b A/D converter and with a Spartan-6 FPGA to accomplish to the following tasks: programming the ASIC internal register and driving the analog to digital conversion of the data. A graphical user interface allows managing the various operations from a PC. A gateway board (not sketched in Fig. 1), once again equipped with a Spartan-6 FPGA, collects all the data coming from the analog-to-digital converter (ADC) board and sends them to PC via Ethernet link. Optical links are used to transfer the data from ADC board to the gateway board. The DAQ used in this paper has been developed by Mediso Medical Imaging Systems within the INSERT project [58].

Each ASIC is placed on an ASIC board, which is connected to SiPMs through a support motherboard that hosts a temperature readout circuit with a standard Wheatstone bridge for Pt100 sensor conditioning.

A powerboard has been designed to provide from an external 12 V the bias voltage required for electronics (3.3 V), and the high voltage for SiPMs with the possibility to set the biasing from 0 up to 50 V. The high voltage is programmable by a DAC with 12-b resolution that is controlled by a microcontroller. The microcontroller also implements a SiPM gain stabilization loop, explained in Section III-D. It is controlled by a LabVIEW interface through USB connection.

All the components of the detection module are shown in Fig. 4, which shows a photograph of the realized prototype for the 2" × 2" $LaBr_3$:Ce readout. All the parts except for the powerboard and the gateway board, not shown in the photograph, are placed inside a shielded box to create dark conditions. The powerboard is connected to the motherboard through a flat cable that brings biasing and temperature information. ASIC boards are placed on the bottom side of the motherboard and not displayed in the photograph.

D. SiPM Gain Stabilization Strategy

The temperature compensation is based on a feedback loop controlled by a microcontroller which stabilizes the gain of the SiPMs sensing the temperature of the detectors. In fact, this prototype does not include temperature stabilization by a cooling unit. The low DCR of NUV-HD SiPMs allows working at room temperature without an evident worsening of performances, differently from other kind of detectors like SDDs [26]. The SiPM gain is given by [20], [59]

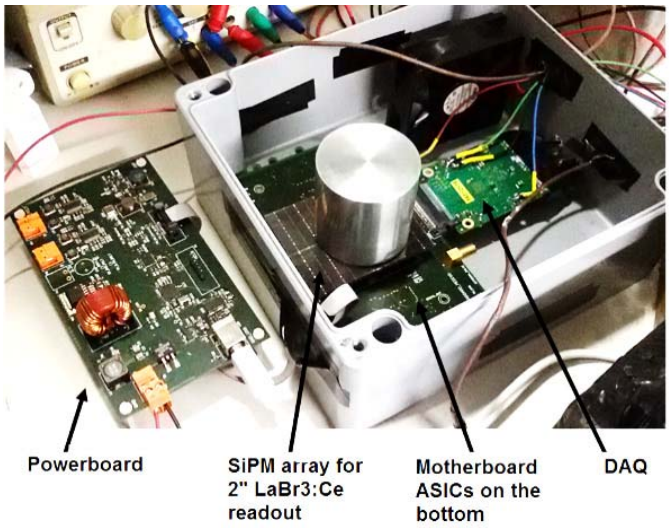

Fig. 4. Photograph of the realized detection module prototype for 2" $LaBr_3$:Ce spectroscopy.

$$G_{\mathrm{SiPM}} = \frac{C_{\mathrm{SiPM}} \cdot (V_{\mathrm{bias}-} V_{\mathrm{BD}})}{q} \tag{6}$$

where G_{sipm} is SiPM gain, C_{sipm} is the capacitance of a single microcell, V_{bias} is SiPM biasing voltage, and V_{BD} is the SiPM breakdown voltage. The difference between the biasing voltage and the breakdown voltage is the overvoltage (OV). Since the breakdown voltage changes with temperature, we implemented a control loop that adjusts the SiPM biasing voltage (V_{bias}) sensing the temperature on the photodetectors array (T_{meas}) and comparing it with a reference temperature (T_{ref}) set to 25 °C, according to the following equation:

$$V_{\mathrm{bias}} = V_{\mathrm{ref}} + \frac{dV_{\mathrm{BD}}}{dT} \cdot (T_{\mathrm{meas}-} T_{\mathrm{ref}}). \tag{7}$$

The coefficient of breakdown voltage variation with temperature (dV_{BD}/dT) of the devices was measured by FBK and it is equal to 26 mV/°C, linear in the temperature range of interest (from 10 °C up to 40 °C). This value is competitive with other commercial SiPM [60]. Since the breakdown voltage is uniform for all the SiPMs of the array, the loop gives the same biasing voltage to all the photodetectors. The temperature information is given by a Pt100 sensor placed on the bottom of the SiPM array that is conditioned by a standard Wheatstone bridge placed on the motherboard.

The loop can operate in real-time during measurements and can adjust the biasing voltage with a frequency programmable from a LabView interface. In all the measurements presented in this paper, the SiPM gain stabilization loop was active and set to adjust the SiPMs' bias every second. Its optimization and validation can be found in [61]. Energy spectra of ^{137}Cs were acquired irradiating the 1" × 1" crystal with the temperature

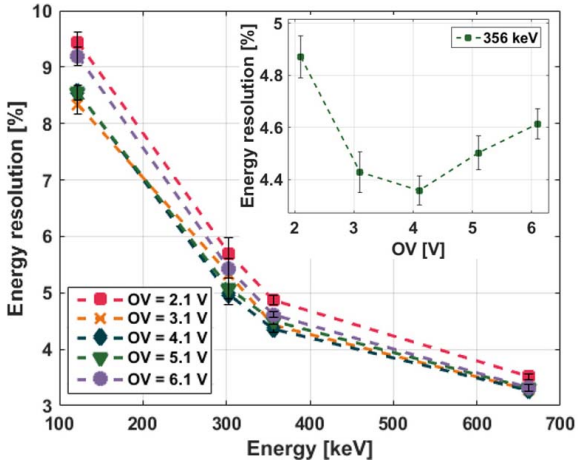

Fig. 5. Energy resolution versus energy at different SiPM OVs. It is also reported that the energy resolution of the 356-keV energy peak at different OVs is 4.1 V. Measurements were performed at 30 °C.

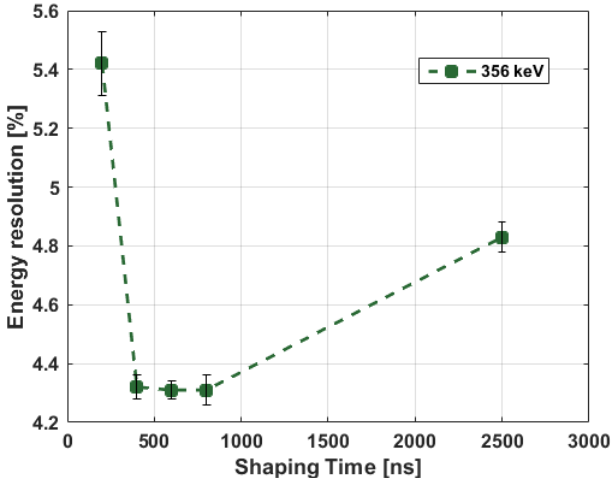

Fig. 6. Energy resolution of the 356-keV energy peak at different electronics shaping times. The optimum is 800 ns. Measurements were performed at 30 °C.

changing from 25 °C to 30 °C without and with the activation of the loop. Looking at the position of the 662-keV peak in ADC channels, the loop allowed decreasing the maximum shift of the peak respect to its initial position at 25 °C from 5% without the loop to 0.45% with the loop in the considered temperature range. The residual shift is due to a nonperfect measurement of the SiPMs' temperature by the Pt100 sensor that is placed on the bottom side of the SiPMs' board and not in contact with SiPMs.

IV. Experimental Results

A. Optimization of Operating Voltage and Shaping Time

A study of the energy resolution at different SiPM OVs and at different electronics shaping times was performed to select the optimal operating parameters.

We present the results with the 2" × 2" $LaBr_3$:Ce crystal, but a similar analysis was performed with the 1" × 1" $LaBr_3$:Ce achieving comparable results.

Measurements were performed irradiating the 2" crystal separately with uncollimated ^{57}Co (122 keV), ^{133}Ba (303 keV, 356 keV), and ^{137}Cs (662 keV) sources. The energy resolution of the four energy peaks was evaluated at OV ranging from 2.1 to 6.1 V with a step of 1 V at a temperature of 30 °C, and the results are shown in Fig. 5. The lowest value of energy resolution corresponds to the optimum operating voltage that represents the best compromise between ENF, DCR, PDE, and SiPM gain M. It was found 4.1 V of optimum OV for all the energy peaks, except for the 122-keV energy where the lower value of energy resolution is at 3.1 V. The deviation is within the margin of error presented in the graph. The error is due to the 95% confidence intervals of the Gaussian fitting used for the estimation of the energy resolution.

It is rather evident that with increasing energy, the relative difference in terms of energy resolution at different OV decreases. In fact, considering the same increment in terms of ENF, DCR, and PDE with OV, a larger number of photoelectrons proper of high-energy gamma rays keep smaller the respective statistical and noise contributions with respect to the intrinsic contribution.

Fig. 6 reports the energy resolution of the 356-keV energy peak at different electronics shaping times (200, 400, 600, and 800 ns, and 2.5 μs) with the step allowed by the ASIC. Measurements were performed at 30 °C. The optimum shaping time is 800 ns. This value is coherent with a trade-off between a complete integration of the SiPM signal and the integration of the noise. In fact, considering the involved time constants, the signal entering in one ASIC channel has a time duration as a result of a convolution of three exponentials. The first one is related to the 16 ns of $LaBr_3$:Ce decay time constant. The second is the 60 ns of SiPM microcells recovery time. The last is about 50 ns for the parallel between the input impedance of the ASIC (ten of Ohm) and the output capacitance of SiPM (∼2.5 nF).

B. Gamma-Ray Spectroscopy With 2" × 2" $LaBr_3$:Ce

Extensive measurements were performed by irradiating the 2" × 2" $LaBr_3$:Ce crystal simultaneously with uncollimated ^{57}Co (122 keV), ^{133}Ba (303 keV, 356 keV), ^{137}Cs (662 keV), and ^{60}Co (1173 keV, 1333 keV) sources. The gain of the ASIC was set to properly acquire the spectra of these five energies that represent the lowest limit of interest for the application [1]. It was not possible to acquire higher energy gamma transitions with the same electronics gain due to the limited dynamic range of the ASIC which was developed for 140 keV (^{99}Tc) of SPECT.

For each event, the signals provided by the 72 SiPMs covered by the crystal were added to create the gamma-ray spectra to be analyzed. Since, the ASIC channels were tested to check the gain homogeneity and the SiPMs in the array were chosen to be uniform in terms of breakdown voltage, no additional calibrations were applied.

Fig. 7 presents the gamma-ray energy spectra of the four radiation sources. They were acquired at OV = 4.1 V, a shaping time of 800 ns, and at a room temperature of 30 °C

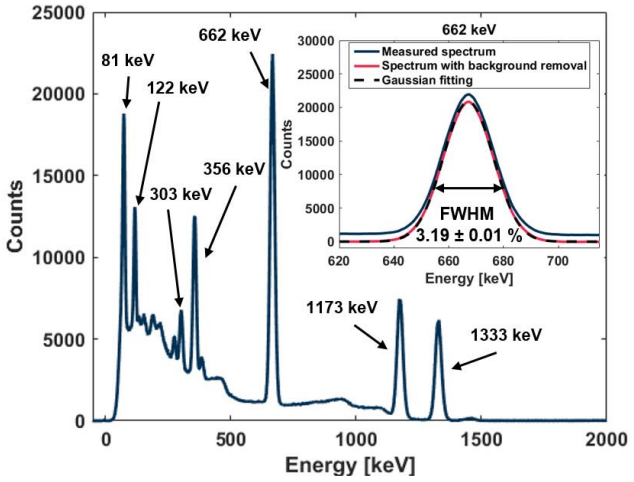

Fig. 7. Best energy spectra acquired irradiating the 2" $LaBr_3$:Ce with ^{57}Co (122 keV), ^{133}Ba (81 keV, 303 keV, 356 keV), ^{137}Cs (662 keV), and ^{60}Co (1173 keV, 1333 keV) sources. Measurements were performed with an OV of 4.1 V, 800 ns of shaping time, at 30 °C. Inset: an energy resolution of 3.19 ± 0.01 was achieved at 662 keV.

(the prototype does not implement a temperature stabilization strategy, i.e., with the use of Peltier cells). The properties of the tested crystal are preserved as temperature increases: the light output of $LaBr_3$:Ce crystal changes less than 1% in the range of 0 °C to +55 °C [4]. The SiPM gain was stabilized by the loop explained in Section III-D, adjusting the biasing voltage every second. The measured resolution of 3.19% full-width at half-maximum (FWHM) at 662 keV (see the inset in Fig. 7) is, to our knowledge, the best value for a large $LaBr_3$:Ce readout by SiPMs. Fig. 8(a) shows the positions in channels ADC of the six energy peaks which are used for the energy calibration with the linear fitting. Fig. 8(b) shows the fitting residuals estimated as [11]

$$\text{Fitting Residual } [\%] = \frac{\text{Expected} - \text{Observed}}{\text{Expected}}. \qquad (8)$$

It is important to note that the residual estimation of (8) can be used in this framework because $LaBr_3$:Ce has a proportional response in the tested energy range (from 122 keV to 1.33 MeV) [13]. In other cases, the equation must consider the nonproportionality of the scintillator.

Excluding the residual at 122 keV, most probably affected by ANGUS nonlinearity for small signals, the residuals show a maximum linearity error of 0.8% at 662 keV. Therefore, we can assume that in this energy range the SiPMs have a linear response. Since, we are in the case of a dead time of SiPM microcells (60 ns) longer then the decay time of the crystal (16 ns), the assumption of linear response can be verified putting the number of microcells into the standard formula of the SiPM saturation [62]

$$N_{\text{fired}} = N_{\text{total}} \cdot \left(1 - e^{\left(-\frac{N_{\text{phe}}}{N_{\text{total}}}\right)}\right) \qquad (9)$$

where N_{fired} is the number of fired microcells, N_{total} is the total number of microcells covered by the crystals, N_{phe} is the number of detected photons or photoelectrons. N_{phe} is

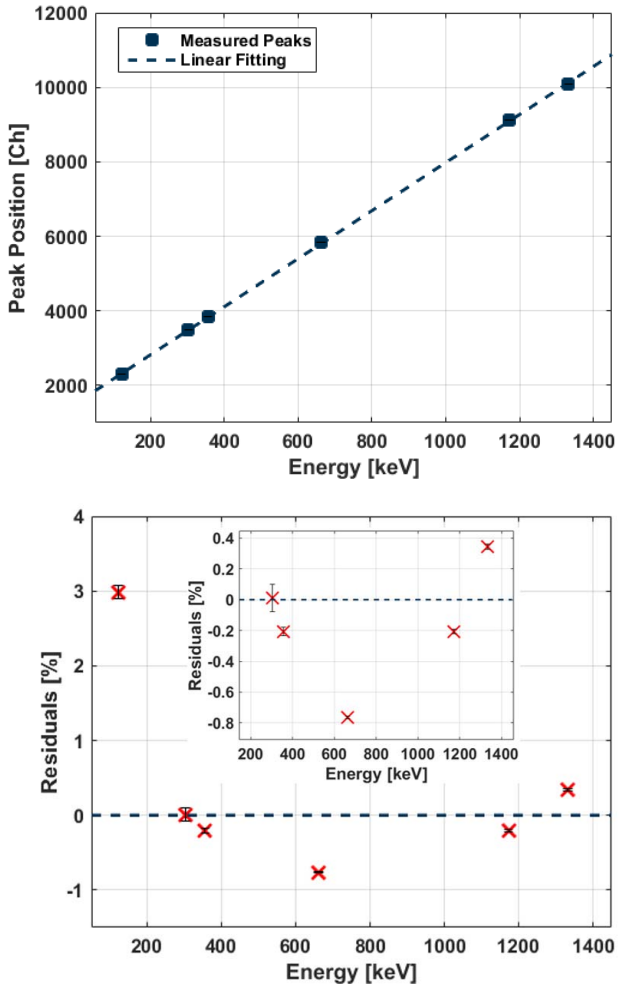

Fig. 8. (a) Linear fitting of photopeak energy measured in ADC channels versus the corresponding energy in kiloelectron volt. Error bars are not visible because they are mostly included in the data points. (b) Percentage residual error in linear fitting. Zoomed-in view of the residuals between 300 and 1300 keV is also shown. Error bars are also reported, and they are mostly included in the data points.

given by the number of incident photons N_{ph} converted by the PDE. N_{phe} takes into account also the crosstalk contribution to the signal, which can be described with the crosstalk probability P_{CT}

$$N_{\text{phe}} = N_{\text{ph}} \cdot \text{PDE} \cdot (1 + P_{\text{CT}}). \qquad (10)$$

Referring to (2), the number of incident photons N_{ph} can be estimated starting from the energy of the gamma-ray, the light yield of the crystal and the collection efficiency η_c. The collection efficiency is the unknown parameter. Its estimation was done reading the amplitude of the merged signals of the 72 SiPMs on the 50-Ω input resistor of a digital 12-b oscilloscope (Lecroy WaveRunner HRO64zi). The efficiency was the ratio between the measured amplitude of the voltage signal on the oscilloscope and the expected amplitude estimated at fixed energy and considering a collection efficiency of 100%. For the estimation of the expected amplitude we use the values of PDE and SiPM gain listed in Table II. The estimated value of collection efficiency was 70% and it is used for the following evaluations.

TABLE II

LaBr$_3$:Ce, SIPM, AND ELECTRONICS PARAMETERS USED FOR THE ESTIMATION OF THE THREE CONTRIBUTIONS OF THE ENERGY RESOLUTION

Parameter	Value
Y [4]	63 ph/keV
η_c	70 %
PDE (OV = 4.1 V, 380 nm)	38 %
ENF (OV = 4.1 V)	1.13
M (OV = 4.1 V)	$1.5 \cdot 10^6$
DCR (OV = 4.1, T = 30°C)	140 kcps/mm^2
Cell density	1100 cells/ mm^2
Cross-talk probability (OV = 4.1)	10 %
ENC series and 1/f	0.6 pC
τ	800 ns
A3	0.25

TABLE III

MEASURED ENERGY RESOLUTION OF GAMMA-RAY PEAKS WITH 2" LaBr$_3$:Ce AND ITS STATISTICAL, NOISE, AND INTRINSIC CONTRIBUTION

Epk [keV]	Rmeas [%]	Rstat [%]	Rnoise [%]	Rintr [%]
122	8.22 ± 0.07	5.54 ± 0.11	2.98 ± 0.05	5.29 ± 0.02
303	4.72 ± 0.07	3.51 ± 0.07	1.20 ± 0.02	2.92 ± 0.03
356	4.30 ± 0.02	3.24 ± 0.07	1.02 ± 0.02	2.64 ± 0.04
662	3.19 ± 0.01	2.38 ± 0.05	0.55 ± 0.01	2.05 ± 0.04
1173	2.30 ± 0.01	1.79 ± 0.04	0.31 ± 0.01	1.41 ± 0.03
1333	2.16 ± 0.01	1.68 ± 0.03	0.27 ± 0.01	1.33 ± 0.03

Thus, considering the maximum measured energy of 1333 keV, the SiPM parameters reported in Table II, a coupled area equal to the surface of the 2" crystal, the SiPM linearity residual is estimated as

$$\text{Linearity Residual } [\%] = \frac{N_{\text{phe}} - N_{\text{fired}}}{N_{\text{phe}}}. \tag{11}$$

We obtained a residual of 0.6%. Consequently, it is possible to consider the SiPM saturation negligible in this energy range.

The energy resolution of the six energy peaks was estimated as the FWHM of a Gaussian fitting. The peak analyzer tool of Origin software was used for background removal. In Table III are listed the energy resolution R in terms of percentage FWHM for gamma-ray peaks shown in Fig. 7. The error was estimated as the 95% confidence intervals of the Gaussian fitting. A higher value of error for low-energy peaks is due to the background removal that can introduce more uncertainties in the fitting. Table III reports an estimation of the statistical, noise, and intrinsic contributions starting from the equations written in Section I. For the calculation of the statistical and noise contribution, we consider the parameters listed in Table II. All SiPM parameters were quoted at the OV of 4.1 V. They were measured by FBK with the automatic procedure explained in [62]. Knowing the DCR of 52 kcps/mm^2 measured at 20 °C, we estimated a DCR of 140 kcps/mm^2 at 30 °C, which was used for the estimation of the parallel term of the ENC with (5). The parameter ENC series and $1/f$ listed in Table II represents an estimation of the sum of the ENC due to the series and the $1/f$ noise of ANGUS that was designed to provide a low-noise front-end electronics. The total ENC used for the estimation of R_{noise} was obtained summing the contributions with (4). The intrinsic contribution was quoted inverting (1) knowing R_{meas} and the other contributions. $A3$ is the shaper constant of an RC filter, while τ is the shaper constant.

The impact of the crosstalk on dark events has been evaluated to verify the suitability of the use of just an average DCR for the parallel noise estimation with (5). For instance, in the worst case at 122 keV, the parallel noise term is 1.55% considering a 10% crosstalk probability and 1.48% taking the average DCR. The difference is negligible with respect to other contributions.

The same crystal was coupled with a Super Bialkali PMT (Hamamatsu R6233-100) by means of the same BC-630 silicone optical grease used with SiPMs. The crystal was irradiated simultaneously with uncollimated ^{133}Ba (356 keV), ^{137}Cs (662 keV), and ^{60}Co (1173 keV, 1333 keV) sources. Signals were amplified with a TENNELEC Tc244 shaping amplifier setting a 250 ns shaping time. An energy resolution of 3.85 ± 0.18%, 3.07 ± 0.03%, 2.17 ± 0.09%, and 2.13 ± 0.04% were achieved at 356, 662, 1173, and 1333 keV, respectively, adopting the same fitting method described for SiPM. The value at 662 keV is coherent with the tabled 3.1% in the Saint Gobain datasheet and close to the experimental results with SiPM. A detailed analysis of the comparison between SiPM and PMT performances is provided in Section V.

TABLE IV

MEASURED ENERGY RESOLUTION OF GAMMA-RAY PEAKS WITH 1" LaBr$_3$:Ce AND ITS STATISTICAL, NOISE, AND INTRINSIC CONTRIBUTION

Epk [keV]	Rmeas [%]	Rstat [%]	Rnoise [%]	Rintr [%]
122	8.39 ± 0.01	5.54 ± 0.11	1.75 ± 0.03	6.05 ± 0.08
303	5.38 ± 0.17	3.51 ± 0.07	0.70 ± 0.01	4.02 ± 0.17
356	5.14 ± 0.06	3.24 ± 0.07	0.60 ± 0.01	3.94 ± 0.03
662	3.70 ± 0.01	2.38 ± 0.05	0.32 ± 0.01	2.81 ± 0.03

C. Gamma-Ray Spectroscopy With 1" × 1" LaBr$_3$:Ce

We also report spectroscopic measurements of 1" × 1" LaBr$_3$:Ce detection module. The crystal was irradiated simultaneously with uncollimated ^{57}Co (122 keV), ^{133}Ba (303 keV, 356 keV), and ^{137}Cs (662 keV) sources. The limited dynamic range of the ASIC did not allow acquiring gamma-ray peaks of higher energy. Measurements were performed with 4.1 V of OV, 800 ns shaping time, at a temperature of 30 °C.

According to (8), the maximum linear fitting residual is 0.8% at 303 keV while the expected SiPM linearity residual at 662 keV, estimated with (11), is 1%.

An energy resolution of 3.70 ± 0.01% FWHM was measured at 662 keV. Table IV shows the estimated energy resolution at all energies and the three estimated contributions, using the same parameters reported in Table II. The collection efficiency of 70% was estimated with the same procedure described in Section IV-B, assuming the same SiPM parameters.

The higher values of energy resolution of the 1" detector with respect to the 2" ones are due to a lower quality of the 1" crystal, most probably associated with a damage in the crystal used, and not to the SiPMs. This damage is quantified with an estimated intrinsic resolution of 2.81% at 662 keV, higher than the 2.05% get for the 2" crystal (Table III). To verify this hypothesis, the 1" × 1" crystal was tested with Hamamatsu R6233-100 PMT achieving an energy resolution of 3.57 ± 0.04% at 662 keV, very close to the measured resolution with SiPMs. The result with the PMT is in line with the estimated intrinsic contribution of 2.81%. In fact, considering the noise contribution of PMT negligible as suggested in [13], assuming a collection efficiency of 90% as reported in [11], a typical variance of the electron multiplier gain of 0.2, and considering a quantum efficiency of 34% as listed in [64], the theoretical energy resolution is 3.62%. This value is the quadratic sum of statistical and intrinsic contribution and it is close to the measured value of 3.57%.

D. Multichannel Versus Merged Readout

The 1" crystal was also tested with a simplified setup. The 25 SiPMs covered by the crystals were merged and readout by the 50-Ω input resistor of a 12-b oscilloscope (Lecroy WaveRunner HRO64zi). The estimated energy resolution of the 662-keV peak is 3.87 ± 0.06%, worse than the 3.70% obtained with the low-noise ANGUS readout.

For the 2" crystal, this simplified measurement approach is not viable due to: 1) the large total capacitance (∼200 nF), which, combined with the 50-Ω input impedance and a time constant of 10 μs, produces a large occurrence of pile-up, limiting severely the count rate and 2) a very small maximum output signal of only 10 mV for a 662-keV photon, poorly resolvable with the oscilloscope ADC resolution. Furthermore, even dark events are affected by the time constant of 10 μs, with a consequent high probability of pile-up which produces a shift of the signal offset. Consequently, the use of a multichannel ASIC for single pixel readout becomes mandatory, in addition to the need for future imaging measurements (which are, however, not within the purposes of this paper). A compact ASIC readout is also required with the increasing of channels covered by larger crystals (i.e., 3.5" $LaBr_3$:Ce).

V. Discussion

To study the reasons of the small difference between SiPMs and PMT spectroscopic performances reported here, it is useful to make a comparison based on the analysis of the three contributions of the energy resolution at different energies. In the following, we limit the analysis to the 2" crystal readout performances.

The contributions of SiPMs are listed in Table III, while Table V shows a similar estimation for PMT. For the statistical column of Table V, we assume to have a collection efficiency of 90% as suggested in [11], a typical variance of the electron multiplier gain of 0.2, and a quantum efficiency of 34% as listed in [64]. The noise contribution of PMT can be neglected as suggested in [13], while we assume to have the same intrinsic contribution estimated from SiPM measurements,

TABLE V

Measured and Estimated Energy Resolution From Statistical and Intrinsic Contribution of Gamma-Ray Peaks of 2" $LaBr_3$:Ce Readout by Hamamatsu R6233-100 PMT

Epk [keV]	Rmeas [%]	Rstat [%]	Rintr [%]	Restim [%]
122	--	5.32 ± 0.13	5.29 ± 0.02	7.50 ± 0.08
303	--	3.38 ± 0.08	2.92 ± 0.03	4.47 ± 0.04
356	3.85 ± 0.18	3.11 ± 0.08	2.64 ± 0.04	4.08 ± 0.08
662	3.07 ± 0.03	2.28 ± 0.06	2.05 ± 0.04	3.07 ± 0.07
1173	2.17 ± 0.09	1.72 ± 0.04	1.41 ± 0.03	2.22 ± 0.05
1333	2.13 ± 0.04	1.61 ± 0.04	1.33 ± 0.03	2.09 ± 0.05

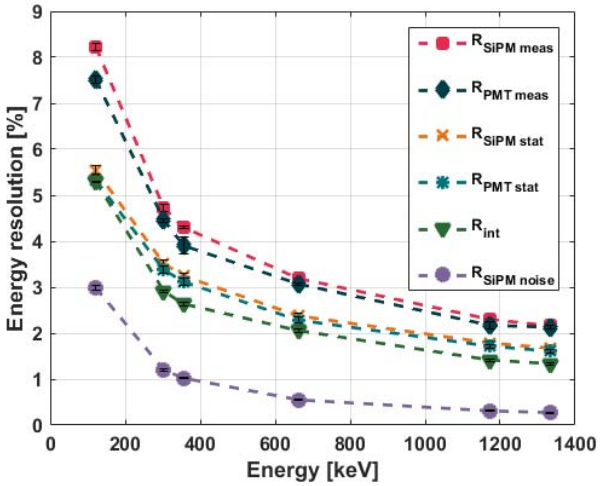

Fig. 9. Comparison of the measured energy resolution and its statistical, noise, and intrinsic terms of 2" $LaBr_3$:Ce readout with SiPM and PMT. For PMT, the points at 122 and 303 keV were just estimated because of the nonavailability of experimental data. Error bars of the measured data are reported and are mostly included in the data points.

since the crystal is the same. From the comparison of the estimated energy resolution at 356, 662, 1173, and 1333 keV reported in the last column with the measured values reported in the first column of Table V, we have a proof of all the previous assumptions because the values are close.

Fig. 9 shows a plot of the measured energy resolution with SiPM array coupled with 2" × 2" $LaBr_3$:Ce at different energies and its estimated three contributions listed in Table III. For PMT, we reported the measured energy resolution for 356, 662, 1173, and 1333 keV peaks, while we put the estimated values for 122 and 303 keV peaks, as listed in Table V. For all the energy peaks, we plot the statistical term listed in Table V.

From the graph, it is evident that the noise term has a negligible impact also at low energy, where the average number of generated electrons is smaller. As a proof, we can estimate the improvements assuming to work at 0 °C. The noise contribution at 122, 303, 356, and 662 keV can be estimated supposing to have the same ENC due to series and $1/f$ noise of 0.6 pC and the ENC due to the parallel contribution estimated from the DCR of 7.17 kcps/mm^2. The noise contribution due to the sum of parallel, series, and

$1/f$ terms is expected to decrease from 2.98% to 2.61% at 122 keV, from 1.20% to 1.05% at 303 keV, from 1.02% to 0.90% at 356 keV, and from 0.55% to 0.48% at 662 keV. The consequent expected energy resolution decreases from 8.22% to 8.09% at 122 keV, from 4.72% to 4.69% at 303 keV, from 4.30% to 4.28% at 356 keV, and from 3.19% to 3.18% at 662 keV. Except for the 122-keV energy peak where an improvement of about 0.1% was predicted, at higher energies no appreciable improvement can be expected. In conclusion, the low DCR of the NUV-HD technology and the low-noise front-end ASIC allow keeping negligible the noise contribution at almost all energies involved in the application.

Therefore, the reason of the gap between the spectroscopic performances of SiPM and PMT readouts is in the statistical term. A direct comparison can be done looking at the result at 662 keV, where 3.19% and 3.07% energy resolutions were measured for SiPM and PMT readouts, respectively. NUV-HD SiPMs and PMT are characterized by a similar quantum efficiency (38% versus 34%), a similar ENF (1.13 versus 1.2), but NUV-HD SiPM has a lower collection efficiency (70% versus 90%) than PMT and this has an impact on the statistical term. The difference can be due to the presence of dead areas in SiPM array which cause an array FF of 90%, while PMTs are characterized by a continuous photosensitive area. In addition, this detector is a prototype and SiPMs and $LaBr_3$:Ce are not encapsulated but simply in contact through optical grease, and some photons can escape from the border.

Finally, at energies higher than 1 MeV, where the average number of generated photoelectrons is higher, SiPM and PMT performances have a smaller difference (2.16% versus 2.13% at 1.33 MeV). This difference may be smaller above 10 MeV, where the average number of generated photoelectrons is so high to make negligible the statistical contribution.

Finally, we note here that the noise term is low enough to avoid a significant deterioration of the performance in the perspective to upgrade the photodetector area to readout larger crystals, i.e., 3.5" diameter $LaBr_3$:Ce.

VI. Conclusion

In this paper, we present a new prototype of a gamma-ray detection module based on new NUV-HD SiPMs for 1" and 2" LaBr3:Ce readout. The 2" module was tested between 122 keV and 1.3 MeV, achieving a very good energy resolution, as 3.19% FWHM at 662 keV. The readout of the same crystal by means of a Super Bialkali PMT (Hamamatsu R6233-100) showed similar results with high-energy gamma-rays (3.07% FWHM at 662keV). For the 1" crystal an energy resolution of 3.70% FWHM was measured with SiPMs at 662 keV, as slightly worse performance with respect to the 2" detector due to an inferior crystal. This assumption was confirmed by the 3.57% FWHM energy resolution measured at 662 keV with the same scintillator coupled to Super Bialkali PMT.

The achieved performances and the analysis of the contributions of the energy resolution lead us to consider the developed SiPM technology now mature to replace the PMT in applications where high-energy resolution is required. As long as new SiPM technology features low noise and similar or even higher quantum efficiency than those of PMT, the trend will evolve decreasing microcells size to improve the dynamic range in the large energy range required in nuclear physics applications.

Acknowledgment

The authors would like to thank Mediso Medical Imaging Systems, Budapest, Hungary for providing the DAQ used in the measurements. They would like to thank J. Agostini and D. Giarrusso for their help during experimental measurements and G. Faes and D. Rucatti from FBK for supporting SiPM production.

References

[1] D. Jenkins, "Novel scintillators and silicon photomultipliers for nuclear physics and applications," *J. Phys.*, vol. 620, no. 1, p. 012001, 2015.

[2] E. V. D. van Loef, P. Dorenbos, C. W. E. van Eijk, K. W. Krämer, and H. U. Güdel, "Scintillation properties of $LaBr_3:Ce^{3+}$ crystals: Fast, efficient and high-energy-resolution scintillators," *Nucl. Instrum. Methods Phys. Res. A, Accel. Spectrom. Detect. Assoc. Equip.*, vol. 486, nos. 1–2, pp. 254–258, Jun. 2002.

[3] *Brillance Scintillators Performance Summary*. Accessed: Apr. 2017. [Online]. Available: https://www.crystals.saint-gobain.com/sites/imdf.crystals.com/files/documents/brillance_performance_summary.pdf

[4] *Saint Gobain Products*. Accessed: Apr. 2017. [Online]. Available: http://www.crystals.saint-gobain.com/products/brillance-labr3-lanthanum-bromide

[5] A. Giaz *et al.*, "Characterization of large volume 3.5×8 $LaBr_3$:Ce detectors," *Nucl. Instrum. Methods Phys. Res. A, Accel. Spectrom. Detect. Assoc. Equip.*, vol. 729, pp. 910–921, Nov. 2013.

[6] F. Birocchi *et al.*, "Position sensitivity of large volume $LaBr_3$:Ce detectors," in *Proc. IEEE Nucl. Sci. Symp. Conf. Rec.*, Oct. 2009, pp. 1403–1405.

[7] D. Weisshaar *et al.*, "$LaBr_3$:Ce scintillators for in-beam gamma-ray spectroscopy with fast beams of rare isotopes," *Nucl. Instrum. Methods Phys. Res. A, Accel. Spectrom. Detect. Assoc. Equip.*, vol. 594, no. 1, pp. 56–60, 2008.

[8] H. J. Wollersheim *et al.*, "Rare ISotopes INvestigation at GSI (RISING) using gamma-ray spectroscopy at relativistic energies," *Nucl. Instrum. Methods Phys. Res. A, Accel. Spectrom. Detect. Assoc. Equip.*, vol. 537, no. 32, pp. 637–657, 2005.

[9] N. Blasi *et al.*, "Position sensitivity in large spectroscopic $LaBr_3$:Ce crystals for Doppler broadening correction," *Nucl. Instrum. Methods Phys. Res. A, Accel. Spectrom. Detect. Assoc. Equip.*, vol. 839, pp. 23–28, Dec. 2016.

[10] F. Quarati *et al.*, "X-ray and gamma-ray response of a 2×2 $LaBr_3$:Ce scintillation detector," *Nucl. Instrum. Methods Phys. Res. A, Accel. Spectrom. Detect. Assoc. Equip.*, vol. 574, pp. 115–120, 2007.

[11] F. G. A. Quarati *et al.*, "High energy gamma-ray spectroscopy with $LaBr_3$ scintillation detectors," *Nucl. Instrum. Methods Phys. Res. A, Accel. Spectrom. Detect. Assoc. Equip.*, vol. 629, no. 1, pp. 157–169, 2011.

[12] M. Moszyński *et al.*, "A comparative study of silicon drift detectors with photomultipliers, avalanche photodiodes and PIN photodiodes in gamma spectrometry with $LaBr_3$ crystals," *IEEE Trans. Nucl. Sci.*, vol. 56, no. 3, pp. 1006–1011, Jun. 2009.

[13] M. Moszyński *et al.*, "Study of $LaBr_3$ crystals coupled to photomultipliers and avalanche photodiodes," *IEEE Trans. Nucl. Sci.*, vol. 55, no. 3, pp. 1774–1780, Jun. 2008.

[14] M. Ciemala *et al.*, "Measurements of high-energy γ-rays with $LaBr_3$:Ce detectors," *Nucl. Instrum. Methods Phys. Res. A, Accel. Spectrom. Detect. Assoc. Equip.*, vol. 608, pp. 76–79, 2009.

[15] I. Mazumdar, D. A. Gothe, G. A. Kumar, N. Yadav, P. B. Chavan, and S. M. Patel, "Studying the properties and response of a large volume (946 cm^3) $LaBr_3$:Ce detector γ-rays with up to 22.5 MeV," *Nucl. Instrum. Methods Phys. Res. A, Accel. Spectrom. Detect. Assoc. Equip.*, vol. 705, pp. 85–92, Mar. 2013.

[16] P. Dorenbos, J. T. M. de Haas, and C. W. E. van Eijk, "Gamma ray spectroscopy with a Ø19×19 mm_3 $LaBr_3$:0.5% Ce^{3+} scintillator," *IEEE Trans. Nucl. Sci.*, vol. 51, no. 3, pp. 1289–1296, Jul. 2004.

[17] A. Giaz *et al.*, "Investigation on gamma-ray position sensitivity at 662 keV in a spectroscopic 3×3 $LaBr_3$:Ce scintillator," *Nucl. Instrum. Methods Phys. Res. A, Accel. Spectrom. Detect. Assoc. Equip.*, vol. 772, pp. 103–111, Feb. 2015.

[18] R. Pani *et al.*, "A novel compact gamma camera based on flat panel PMT," *Nucl. Instrum. Methods Phys. Res. A, Accel. Spectrom. Detect. Assoc. Equip.*, vol. 513, no. 1, pp. 36–41, 2003.

[19] M. N. Cinti *et al.*, "Reliability of high quantum efficiency MA-PMT for spectrometric quality assurance of scintillation imagers," in *Proc. IEEE Nucl. Sci. Symp. Conf. Rec.*, Oct. 2011, pp. 1665–1668.

[20] D. Renker and E. Lorenz, "Advances in solid state photon detectors," *J. Instrum.*, vol. 4, no. 4, p. P04004, Apr. 2009.

[21] H. O. Anger, "Scintillation camera," *Rev. Sci. Instrum.*, vol. 29, no. 1, pp. 27–33, Oct. 1958.

[22] C. Fiorini *et al.*, "The HICAM gamma camera," *IEEE Trans. Nucl. Sci.*, vol. 59, no. 3, pp. 537–544, Jun. 2012.

[23] P. Busca *et al.*, "Experimental evaluation of a SiPM-based scintillation detector for MR-compatible SPECT systems," *IEEE Trans. Nucl. Sci.*, vol. 62, no. 5, pp. 2122–2128, Oct. 2015.

[24] C. Fiorini *et al.*, "Gamma-ray spectroscopy with $LaBr_3$:Ce scintillator readout by a silicon drift detector," *IEEE Trans. Nucl. Sci.*, vol. 53, no. 4, pp. 2392–2397, Aug. 2006.

[25] P. Busca *et al.*, "Development of a detector based on silicon drift detectors for gamma-ray spectroscopy and imaging applications," *J. Instrum.*, vol. 9, p. C05005, May 2014.

[26] A. D. Butt *et al.*, "Development of a detector for gamma-ray spectroscopy based on silicon drift detector arrays and 2″ lanthanum bromide scintillator," *IEEE Trans. Nucl. Sci.*, vol. 62, no. 5, pp. 2334–2342, Oct. 2015.

[27] S. Gundacker *et al.*, "State of the art timing in TOF-PET detectors with LuAG, GAGG and L(Y)SO scintillators of various sizes coupled to FBK-SiPMs," *J. Instrum.*, vol. 11, p. P08008, Aug. 2016.

[28] A. Ferri, F. Acerbi, A. Gola, C. Piemonte, G. Paternoster, and N. Zorzi, "Performance of a 64-channel, 3.2×3.2 cm^2 SiPM tile for TOF-PET application," *Nucl. Instrum. Methods Phys. Res. A, Accel. Spectrom. Detect. Assoc. Equip.*, vol. 824, pp. 196–197, Jul. 2016.

[29] S. David, M. Georgiou, E. Fysikopoulos, and G. Loudos, "Evaluation of a SiPM array coupled to a $Gd_3Al_2Ga_3O_{12}$:Ce (GAGG:Ce) discrete scintillator," *Physica Medica*, vol. 31, pp. 763–766, Apr. 2015.

[30] N. Dinu *et al.*, "SiPM arrays and miniaturized readout electronics for compact gamma camera," *Nucl. Instrum. Methods Phys. Res. Section A, Accel., Spectrometers, Detectors, Assoc. Equip.*, vol. 787, pp. 367–372, Jul. 2015.

[31] I. Perali *et al.*, "Prompt gamma imaging of proton pencil beams at clinical dose rate," *Phys. Med. Biol.*, vol. 59, pp. 5849–5871, Oct. 2014.

[32] N. Otte, "The silicon photomultiplier—A new device for high energy physics, astroparticle physics, industrial and medical applications," in *Proc. SNIC Symp.*, Stanford, CA, USA, Apr. 2006, pp. 1–9.

[33] A. N. Otte *et al.*, "Development of a SiPM camera for a schwarzschild-Couder cherenkov telescope for the cherenkov telescope array," in *Proc. Sci.*, 2015, p. 1023.

[34] J. Biteau, "Characterization of silicon photomultipliers for the cherenkov telescope array medium-sized telescopes," in *Proc. IEEE Nucl. Sci. Symp. Conf. Rec.*, Nov. 2014, pp. 1–3.

[35] D. R. Schaart *et al.*, "$LaBr_3$:Ce and SiPMs for time-of-flight PET: Achieving 100 ps coincidence resolving time," *Phys. Med. Biol.*, vol. 55, no. 7, pp. N179–N189, 2010.

[36] J. P. Schmall *et al.*, "Timing and energy resolution of new near-UV SiPMs coupled to $LaBr_3$:Ce for TOF-PET," *IEEE Trans. Nucl. Sci.*, vol. 61, no. 5, pp. 2426–2432, Oct. 2014.

[37] P. F. Bloser *et al.*, "Testing and simulation of silicon photomultiplier readouts for scintillators in high-energy astronomy and solar physics," *Nucl. Instrum. Methods Phys. Res. A, Accel. Spectrom. Detect. Assoc. Equip.*, vol. 763, pp. 26–35, Nov. 2014.

[38] P. F. Bloser, J. S. Legere, C. M. Bancroft, M. L. McConnell, and J. M. Ryan, "Scintillator gamma-ray detectors with silicon photomultiplier readouts for high-energy astronomy," *Proc. SPIE*, vol. 8859, p. 88590A, Sep. 2013.

[39] G. Llosá *et al.*, "Detector characterization and first coincidence tests of a compton telescope based on $LaBr_3$ crystals and SiPMs," *Nucl. Instrum. Methods Phys. Res. A, Accel. Spectrom. Detect. Assoc. Equip.*, vol. 695, pp. 105–118, Dec. 2012.

[40] S. Seifert *et al.*, "Monolithic $LaBr_3$:Ce crystals on silicon photomultiplier arrays for time-of-flight positron emission tomography," *Phys. Med. Biol.*, vol. 57, no. 8, pp. 2219–2233, 2012.

[41] M. Grodzicka-Kobylka, M. Moszyński, T. Szczęśniak, M. Szawłowski, D. Wolski, and J. Baszak, "MPPC array in the readout of CsI:Tl, LSO:Ce:Ca, $LaBr_3$:Ce, and BGO scintillators," *IEEE Trans. Nucl. Sci.*, vol. 59, no. 6, pp. 3294–3303, Dec. 2012.

[42] M. Grodzicka-Kobylka, M. Moszyński, T. Szczęśniak, M. Szawłowski, and J. Baszak, "Characterization of 4×4 ch MPPC array in scintillation spectrometry," *J. Instrum.*, vol. 8, p. P09020, Sep. 2013.

[43] M. Grodzicka-Kobylka, T. Szczęśniak, M. Moszyński, S. Korolczuk, J. Baszak, and M. Kapusta, "Characterization of large TSV MPPC arrays (4×4 chand 8×8 ch) in scintillation spectrometry," *Nucl. Instrum. Methods Phys. Res. A, Accel. Spectrom. Detect. Assoc. Equip.*, vol. 869, pp. 153–162, Oct. 2017.

[44] A. Ulyanov *et al.*, "Performance of a monolithic $LaBr_3$:Ce crystal coupled to an array of silicon photomultipliers," *Nucl. Instrum. Methods Phys. Res. A, Accel. Spectrom. Detect. Assoc. Equip.*, vol. 810, pp. 107–119, Feb. 2016.

[45] M. Moszyński, "Energy resolution of scintillation detectors," *Proc. SPIE*, vol. 5922, p. 592205, Sep. 2005.

[46] C. Fiorini, "Gamma detectors for spectroscopy and imaging based on scintillators coupled to semiconductor detectors," *Proc. SPIE*, vol. 4141, pp. 97–110, Nov. 2000.

[47] P. Dorenbos, J. T. M. de Haas, and C. W. E. van Eijk, "Non-proportionality in the scintillation response and the energy resolution obtainable with scintillation crystals," *IEEE Trans. Nucl. Sci.*, vol. 42, no. 6, pp. 2190–2202, Dec. 1995.

[48] S. A. Payne *et al.*, "Nonproportionality of scintillator detectors: Theory and experiment. II," *IEEE Trans. Nucl. Sci.*, vol. 58, no. 6, pp. 3392–3402, Dec. 2011.

[49] E. Gatti, P. F. Manfredi, M. Sampietro, and V. Speziali, "Suboptimal filtering of $1/f$-noise in detector charge measurements," *Nucl. Instrum. Methods Phys. Res. A, Accel. Spectrom. Detect. Assoc. Equip.*, vol. 297, no. 3, pp. 467–478, 1990.

[50] *Hamamatsu Optical Sensors*. Accessed: Apr. 2017. [Online]. Available: http://www.hamamatsu.com/us/en/index.html

[51] *Ketek Silicon Photomultipliers*. Accessed: Apr. 2017. [Online]. Available: www.ketek.net/products/sipm/

[52] *SenSL Silicon Photomultipliers*. Accessed: Apr. 2017. [Online]. Available: http://sensl.com/

[53] C. Piemonte *et al.*, "Performance of NUV-HD silicon photomultiplier technology," *IEEE Trans. Electron Devices*, vol. 63, no. 3, pp. 1111–1116, Mar. 2016.

[54] C. Piemonte *et al.*, "Characterization of the first FBK high-density cell silicon photomultiplier technology," *IEEE Trans. Electron Devices*, vol. 60, no. 8, pp. 2567–2573, Aug. 2013.

[55] G. F. Knoll, *Radiation Detection and Measurement*, 3rd ed. Hoboken, NJ, USA: Wiley, 2000, pp. 628–629.

[56] S. Ceruti *et al.*, "Isospin mixing in ^{80}Zr: From finite to zero temperature," *Phys. Rev. Lett.*, vol. 115, no. 22, p. 222502, 2015.

[57] P. Trigilio, R. Quaglia, F. Schembari, and C. Fiorini, "ANGUS: A multichannel CMOS circuit for large capacitance silicon photomultiplier detectors for SPECT applications," in *Proc. IEEE Nucl. Sci. Symp. Conf. Rec.*, Nov. 2014, pp. 1–4.

[58] M. Occhipinti *et al.*, "INSERT project: First results of a MR compatible preclinical SPECT based on SiPM photodetectors," in *Proc. IEEE Nucl. Sci. Symp. Conf. Rec.*, Oct. 2016, pp. 1–4.

[59] *An Introduction to the Silicon Photomultiplier*. Accessed: Apr. 2017. [Online]. Available: http://www.sensl.com/downloads/ds/TN%20%20Intro%20to%20SPM%20Tech.pdf

[60] M. Grodzicka-Kobylka, T. Szczęśniak, and M. Moszyński, "Comparison of SensL and Hamamatsu 4×4 channel SiPM arrays in gamma spectrometry with scintillators," *Nucl. Instrum. Methods Phys. Res. A, Accel. Spectrom. Detect. Assoc. Equip.*, vol. 856, pp. 53–64, Jun. 2017.

[61] G. Cozzi *et al.*, "Development of a SiPM-based detection module for large $LaBr_3$:Ce Scintillators for nuclear physics applications," in *Proc. IEEE Nucl. Sci. Symp. Conf. Rec.*, Oct. 2016, pp. 1–5.

[62] M. Grodzicka-Kobylka, T. Szczęśniak, M. Moszyński, M. Szawłowski, and K. Grodzicki, "New method for evaluating effective recovery time and single photoelectron response in silicon photomultipliers," *Nucl. Instrum. Methods Phys. Res. A, Accel. Spectrom. Detect. Assoc. Equip.*, vol. 783, pp. 58–64, May 2015.

[63] C. Piemonte *et al.*, "Development of an automatic procedure for the characterization of silicon photomultipliers," in *Proc. IEEE Nucl. Sci. Symp. Conf. Rec.*, Oct. 2012, pp. 428–432.

[64] *Hamamatsu PMT Datasheet*. Accessed: Apr. 2017. [Online]. Available: http://www.hamamatsu.com/us/en/R6233-100.html